Design and Analysis of Deterministic Distributed Beamforming Algorithms in the Presence of Noise

I. Thibault*, *Student Member, IEEE,* A. Faridi†, *Member, IEEE,* G. E. Corazza*, *Senior Member, IEEE,* A. Vanelli Coralli*, *Senior Member, IEEE,* and A. Lozano†, *Senior Member, IEEE*

Abstract

This paper presents a new deterministic closed-loop phase-alignment algorithm based on quantized feedback from the receiver for distributed beamforming. In contrast with previously proposed methods, which entailed repeated transmissions from all the nodes in the network, this new algorithm requires each node to transmit only once during the synchronization cycle. This drastically reduces the amount of power consumed to achieve phase alignment, yet the new algorithm converges at least as fast as all other existing schemes. In contrast with previous analyses of distributed beamforming based on random phase updates, where noise had been disregarded, here it is explicitly included in the models and shown to have a considerable effect that cannot be ignored. With and without noise, analytical expressions that characterize the performance of the new algorithm are provided, with emphasis on various limiting regimes of interest.

Index Terms

Distributed Phase Synchronization with Noise, Virtual Arrays, Wireless Sensor Networks

* I. Thibault, G. E. Corazza, and A. Vanelli Coralli are with the Department of Electrical, Electronic, and Information Engineering, University of Bologna, Viale Risorgimento, 2, 40134 Bologna, Italy, emails: {ithibault, gecorazza, avanelli}@arces.unibo.it

† A. Faridi and A. Lozano are with the Department of Information and Communication Technologies, Pompeu Fabra University, Barcelona 08018, Spain. Their work is supported by AGAUR (Catalan Agency for Administration of University and Research Grants), emails: {azadeh.faridi, angel.lozano}@upf.edu

I. Introduction

Distributed beamforming is a cooperative communication technique that enables a cluster of sensors to emulate a virtual antenna array, allowing for directed message delivery to the intended destination. In other words, nodes pool their antenna resources and synchronize their radio transmissions so that they coherently aggregate in a desired direction in space yielding power gains proportional to the number of cooperating devices. Moreover, beampattern shaping is beneficial for reducing interference towards/from unintended terminals, and favors the implementation of Space Division Multiple Access (SDMA) schemes which allow the network to spatially multiplex different streams of data for independent receivers.

A possible application is in wireless sensor networks, which must comply with strict energy-efficient policies with a view on maximizing the system's life span. Sensors are power-restrained devices that survive on limited battery supplies that typically cannot be recharged. Single-node communication happens to be highly inefficient, since the signal transmitted from a typically low-cost isotropic antenna is undirected and, consequently, only a fraction of the transmitted power becomes useful for communication purposes. Moreover, the transceiver is the most power-consuming element in a sensor, thus a more efficient use of this resource is desirable. Under these circumstances, collaboration comes as a compelling solution when a common message, usually the result of a sensing campaign, must be relayed to a receiver. Potential gains achievable with distributed beamforming, in fact, enable cooperating sensors to back off their powers when transmitting information.

Clearly, for a cluster of distributed nodes, emulation of a virtual array is not trivial. As opposed to a centralized scenario, where all elements naturally share a common phase and frequency reference, and a regular geometry guarantees tight control on the relative phase shifts, this distributed setup faces new challenges. Each node has its own, independent local oscillator with random initial phase as well as phase noise, and sensor locations are typically unknown. Distributed phase-alignment procedures are thus required in order for the network to be able to steer a beam in the desired direction in space. This scenario has attracted the attention of

many researchers, that have tackled various aspects of this problem from different perspectives by designing algorithms for phase alignment [1]–[22], by studying the properties of average beampatterns created by nodes randomly distributed in space through the theory of random arrays [23]–[28], and by providing node selection procedures that sort transmitters on the basis of their mutual phase alignment to efficiently create an array out of a useful subset of nodes [29]–[32].

A. State of the Art

All works in [1]–[22] tackle the phase alignment issue for successful beam steering. They evaluate the performance in terms of the improvement of the Received Signal Strength (RSS), i.e., the intensity of the useful part of the aggregate signal at the receiver, as the distributed synchronization procedure unfolds. In other words, the aim of these algorithms is to enable the network to steer a beam in the desired direction in space by successively adjusting the phase of the transmitted signals according to the policy dictated by the algorithm. Clearly, the faster the received signals achieve coherence, the better in terms of energy consumption since less signaling is required for synchronization.

In [1]–[4] a closed-loop, distributed, and iterative phase synchronization procedure, called Random 1-Bit Feedback (R1BF) algorithm, is presented. Nodes apply, independently from one another and simultaneously, random phase adjustments to their signals. On the basis of one bit of feedback from the receiver, which informs the network if the set of random perturbations has improved or worsened the RSS, the nodes decide whether to maintain or discard the introduced phase shifts. This randomized process is carried out until the received phases achieve a desired level of coherence. Authors in [1] show that, for a wide variety of probability distribution functions (PDFs) for the phase adjustments, the procedure leads to asymptotic coherence with probability one. An analytical framework is provided in [5] to analyze the convergence of the R1BF algorithm by considering it as a random search algorithm. In [6] and [7], a signed variation of the R1BF algorithm is introduced to improve convergence: if nodes receive a negative feedback, they change the sign of the tested phase shifts and apply them before starting a new test.

A further enhancement of this method is described in [8], where, in case of positive feedback, the nodes insist on applying the successful shift until the signal starts worsening again, and in case of negative feedback, they adopt the same strategy but by inverting the sign of the shift. In [9] this application is extended to a multiuser scenario, where M separate clusters of nodes have to communicate with M distinct receivers. In this work, distributed beampattern shaping is used to implement SDMA schemes: the network is divided into M sub-clusters of nodes that have to multiplex M independent streams of data to M non-cooperating receivers. New versions and improvements of R1BF are also contained in [18]–[20]. A feedback based synchronization procedure is also introduced in [10]. Here, the received signal is considered as composed by a sum of complex signals, each one relative to the aggregate transmissions from a sub-cluster of nodes. The receiver estimates the magnitude and the phase of the signals relative to each cluster, and the objective is to align these signals in phase. As opposed to the R1BF algorithm, the feedback is based on the complex signal, and not only on the magnitude, and it is directed to subsets of nodes.

In our previous works, [21], [22], with a view on reducing the time to synchronize with respect to the random approach, we proposed an iterative closed-loop procedure, still based on quantized feedback from the receiver, but built on a deterministic phase update strategy. In this approach, nodes take turns in performing phase tests, and they are only allowed to test a particular number of predefined phase shifts. The receiver performs successive RSS measures for each node (one for every possible phase adjustment), and sends a bit of feedback for each of these measurements. The node will then apply the phase shift that has yielded the best RSS improvement. Simulation results provided in [21], [22] show how the deterministic strategy outperforms the random one in terms of convergence time both in static and time-varying channel environments.

Other relevant contributions in this area are [11]–[17]. A time-slotted closed-loop procedure for carrier synchronization is presented in [11] and [12]. An interesting blind zero-feedback distributed beamforming is presented in [13]. Here, the natural misalignment of the carriers is exploited to reach a suitable set of beamforming gains. A half duplex amplify and forward relay network is considered in [14]: an adaptive beamforming scheme based on predefined sets of

deterministic perturbations of the beamforming weights driven by a one-bit feedback from the receiver is presented. Authors in [15] analyze the problem of distributed beamforming from an information-theoretic point of view, providing a lower bound for the time required to achieve phase coherence at destination in a binary signaling case. In [16], a method for carrier phase and frequency synchronization is presented in case of a two-transmitter cooperation scheme. It is shown how this method is also robust to mobility of the terminals. In [17] a closed-loop phase tracking routine based on Code Division Multiple Access is proposed to achieve coherent combining of signals transmitted from a cluster of distributed antennas. The effect of partitioning the transmitted energy between synchronization symbols and data packets is investigated, by observing its impact on the data bit error rate. In addition, practical implementations of distributed beamforming have been proven to be effective, [33], feasible, and implementable on commodity hardware with low-quality oscillators [34].

B. Our Contribution

Our focus is on distributed synchronization schemes that rely on a low-rate quantized feedback from the receiver [1]–[10]. Surprisingly, given that the defeat of noise is the main driver of distributed beamforming, the impact of noise in these schemes has been ignored. The first attempt to consider the impact of noise has been made in [35], but this analysis does not quantify the actual performance of these schemes when the synchronization process is hindered by this impairment. In this work, noise is incorporated into the model and shown to have a considerable effect that simply can not be ignored.

A new algorithm, more energy-efficient than its predecessors , is proposed and its performance is analytically characterized, with and without noise. Comparisons with existing alternatives are also provided, with and without noise. Specifically:

- We put forth a new deterministic algorithm that relies on low-rate feedback to successively align the phases of the transmitters to an arbitrary bias selected by the receiver. This algorithm converges faster than existing random schemes and with less energy consumption than previous deterministic solutions.

- The performance of the new algorithm is analytically characterized in the absence of noise. This characterization enables bench-marking against previous random solutions, which were all evaluated only in noiseless conditions.
- The analytical characterization of the new algorithm is extended to incorporate the impact of noise, with emphasis on the low- and high-power regimes. The former embodies the conditions in which a distributed beamforming system would most likely have to operate whereas the latter serves as a bridge with the noiseless analysis. The analysis sheds light on the interplay between the number of sensors, the signal-to-noise ratio (SNR), and the feedback rate.
- The performance of the new algorithm is compared against that of random schemes. Since the analysis of random schemes appears unwieldy in the face of noise, the performance is determined via Monte-Carlo.

The remainder of the manuscript is organized as follows: the general system model is described in Section II, the random noiseless synchronization approach is illustrated in Section III, and Section IV describes the deterministic synchronization procedure. The analytical insights related to the latter are provided in Section V both in the absence and presence of noise (in Section V-A and Section V-B, respectively). Finally, Section VI features a comparison between the new algorithm and the random one and Section VII concludes the paper.

II. General System Model

In the next sections, we will be discussing two synchronization algorithms, the R1BF algorithm from [1] and our proposed algorithm. In this section, we present the general system model that is common to both algorithms. We will then adapt this model to each particular algorithm in its corresponding section.

The following assumptions are made, in line with previous works on phase synchronization:

- Nodes are unaware of their own locations, of the position of the receiver, and of channel-state information (CSI).
- All devices are equipped with an isotropic antenna.

- All sensors transmit at the same power.
- Since the receiver's distance is considered to be much greater than the radius of the network itself, path losses are considered to be the same for all nodes.
- There is no multipath and thus the effect of the channel amounts to a phase rotation, random and static for each node. This could represent, for instance, situations where the receiver is a satellite or an elevated cell site[1].
- All nodes are locked to the same carrier frequency f_{c}, and frequency drift is considered negligible[2]. Hence, the phase shift of each local oscillator is also static and modeled as uniform in $[0, 2\pi)$.
- Sensors share a common time reference, i.e., time synchronization is present throughout the whole network.

In order to steer a beam towards the receiver, each transmitter should multiply its signal by an appropriate complex beamforming weight to compensate for both the channel rotation and the misalignment due to the local oscillator's phase offset. If each node had access to global CSI, the optimal beamforming weights could be locally computed and the signals would perfectly align in the target direction. In a distributed setup however, obtaining full CSI may not be feasible. To bypass this obstacle, we consider iterative closed-loop synchronization procedures where each transmitter can locally adjust the phase of its signal based on a low-rate feedback it receives from the destination. The phase adjustment is equivalent to multiplying the signal by a complex, unit-magnitude beamforming coefficient with a properly-selected phase. The type of feedback and the type of local phase adjustments depend on the chosen synchronization protocol.

Let N_{a} be the number of active devices in a given time-slot. The channel phase rotation and

[1]This assumption can be relaxed, since the results are still valid when static fading is introduced in the model. Its impact translates into a static offset of the average beamforming gain with respect to the equal gain combining case, which depends on the statistics of the considered fading distribution.

[2]A frequency offset will actually be present, and this translates into a maximum time window within which phase coherence can be assumed to be maintained. Loss of coherence has a detrimental effect on the beamforming gain, and this calls for re-synchronization. This thus becomes a requirement on maximum convergence time [21].

the phase offset of the local oscillator for node i are absorbed into a single variable, ψ_i. In turn, the phase rotation that each transmitter has applied to its signal at time t is denoted by $\phi_i[t]$. During synchronization, nodes transmit unmodulated carriers (beacons), so the complex signal at the receiver is given by

$$r(t) = e^{j2\pi f_c t} \sum_{i=1}^{N_a} e^{j(\psi_i + \phi_i[t])} + n(t) \tag{1}$$

where $n(t)$ is a complex Gaussian random variable, with mean zero and variance σ^2, representing the noise at time t. The value of N_a is fixed throughout the synchronization.

After down conversion and sampling, at the end of time slot m the resultant complex vector relative to the useful signal is

$$\mathcal{R}[m] = \sum_{i=1}^{N_s[m]} e^{j(\psi_i + \phi_i[m])} \tag{2}$$

where $N_s[m]$ is the number of nodes that have been synchronized up to time slot m. The only component in this expression that is locally tunable by each transmitter is the phase of the beamforming weight. The RSS at the end of time slot m, given the superposition of $N_s[m]$ carriers, is simply

$$|\mathcal{R}[m]| = \left| \sum_{i=1}^{N_s[m]} e^{j(\psi_i + \phi_i[m])} \right|. \tag{3}$$

We define the RSS normalized to the total number of nodes N in the network as

$$|\hat{\mathcal{R}}[m]| \triangleq \frac{|\mathcal{R}[m]|}{N} \tag{4}$$

and we dub it normalized RSS (NRSS). The NRSS is maximized when $\psi_i + \phi_i[m] = \Upsilon[m],\ \forall i$, where $\Upsilon[m]$ is an arbitrary constant. The objective is to adjust $\phi_i[m]$ in order to obtain an optimal set of beamforming weights that result in received signal phases that are as close as possible to this condition of coherence.

III. Noiseless Random Distributed Beamforming

The authors in [1] present a random procedure for phase synchronization, called R1BF, ignoring the noise term in (1). According to an iterative paradigm, at the beginning of each time slot, all sensors simultaneously apply a random and independent phase adjustment to their carriers. On the basis of a one-bit feedback from the receiver, they decide whether to maintain or discard the introduced phase shifts: the feedback is a *"keep"* signal if the set of phase adjustments has improved the RSS, or a *"discard"* signal otherwise.

Assuming $\phi_i[m-1]$ is the best known carrier phase at the ith sensor at time slot m, each transmitter applies a random phase adjustment denoted as $\delta_i[m]$, taken from a predetermined PDF $f_{\delta_i}(\cdot)$, striving for a potentially better phase. The applied phase increments are independent over time and across nodes. The tested phase for the ith node at time slot m is then

$$\phi_i^{\text{test}}[m] = \phi_i[m-1] + \delta_i[m]. \tag{5}$$

The corresponding RSS, $|\mathcal{R}[m]|_{\text{test}}$, is given by (3), replacing $\phi_i[m]$ with $\phi_i^{\text{test}}[m]$ and $N_{\text{s}}[m]$ with N. The receiver measures $|\mathcal{R}[m]|_{\text{test}}$ and sends a feedback signal indicating whether the introduced phase shifts have improved the quality of the signal or not, i.e., if $|\mathcal{R}[m]|_{\text{test}}$ is greater or smaller than $|\mathcal{R}[m-1]|$, which is the best value for the RSS up to time slot m. The update process for $\phi_i[m]$ can be summarized as follows:

$$\phi_i[m] \;=\; \begin{cases} \phi_i^{\text{test}}[m], & |\mathcal{R}[m]|_{\text{test}} > |\mathcal{R}[m-1]| \\ \phi_i[m-1], & |\mathcal{R}[m]|_{\text{test}} \leq |\mathcal{R}[m-1]| \end{cases} \tag{6}$$

The value for the record of the best observed RSS is also updated as

$$|\mathcal{R}[m]| = \max\left(|\mathcal{R}[m]|_{\text{test}}, |\mathcal{R}[m-1]|\right) \tag{7}$$

This procedure is iterated and stops only once the RSS has reached a particular threshold value. Phase synchronization is thus achieved in a completely distributed fashion. No network coordination is required, and the receiver only has to estimate the strength of the aggregate of all the signals.

In [1], authors develop an analytical framework to characterize the behavior of the RSS as R1BF takes place. This elegant analysis considers the setting described in Section II, where carriers are synchronized in frequency, with constant (but unknown) phase offsets between transmitters, and constant (but unknown) channel gains. The distributed random adaptation of the phases is shown to converge to coherence with probability one, for a vast range of perturbation distributions, and the dynamics of the algorithm are established. This analysis, however, completely disregards the impact of noise in the convergence.

IV. Deterministic Distributed Beamforming

We here introduce a new energy-efficient phase synchronization procedure, which belongs to the family of deterministic algorithms [21], and which we denote as Successive Deterministic Distributed Beamforming (SDDB). The power consumption due to signaling for phase alignment is drastically reduced with respect to R1BF and to previous deterministic solutions. In this algorithm, sensors transmit successively and independently from one another and the receiver is thereby able to estimate each node's signal separately. Each sensor only wakes up during its assigned time slot to perform synchronization, while all the others remain in power-saving mode. The goal for the receiver is to align the useful part of each received signal as closely as possible to an arbitrary phase bias. Without loss of generality, we can set this phase bias to be zero. The objective of the receiver is then to align the signals of all nodes to the real axis. The procedure stops after N slots, i.e., when all nodes have synchronized. Ideally, if an infinite number of bits were available for the feedback, the receiver could inform each node which exact phase shift to apply to align perfectly to the real axis. We will show that, in the absence of noise, with as few as two bits of feedback (i.e., with four possible phase shifts), beamforming gains within 1 dB of the maximum can be achieved. As mentioned earlier, this approach drastically reduces the power consumption for the training procedure with respect to R1BF and to previous deterministic solutions. In the latter cases, in each time slot, $N_{\mathrm{a}} = N$, i.e., all sensors are always active and transmitting beacons. These schemes potentially allow for cooperative transmission of information even during the synchronization procedure, and they are potentially more adaptive

to time-dependent phase drift due to channel variations or oscillator dynamics, but have larger energy overhead. In SDDB, the synchronization stage and the cooperative transmission stage are disjoint, but $N_{\text{a}} = 1$ in each time slot, meaning that network power consumption per time slot is reduced by a factor of N.

Each node is entitled to apply one phase shift, out of a predefined deterministic set of possible values, which depends on the number of feedback bits available. We identify this set as

$$\mathcal{S}_K = \left\{ k \times \frac{2\pi}{K},\ k = 0, \ldots, K-1 \right\} \tag{8}$$

where K is the number of possible phase shifts, assumed to be a power of two, i.e., $K = 2^b$ where b is the number of bits available for feedback. Alternatively, we can construct $\mathcal{W}_K$, the set of all possible beamforming weights for a given K, as follows:

$$\mathcal{W}_K \triangleq \left\{ w_k = e^{j\, k \frac{2\pi}{K}},\ k = 0, \ldots, K-1 \right\}. \tag{9}$$

Without loss of generality, we can assume that nodes get activated in the same order as their assigned index, i.e., at time slot m, the mth node is the active node transmitting its beacon to the receiver. The receiver then observes

$$r[m] = e^{j\psi_m} + n[m] \tag{10}$$

which is the down-converted and sampled version of the received signal defined in (1), when $N_{\text{a}} = 1$. Since we are focusing on the feedback decision in one particular time slot, which is independent from all other time slots, for simplicity of notation we drop the index m. Denoting the useful part, i.e., the noiseless part, of the complex received signal by v, the received signal r can be rewritten as

$$r = v + n. \tag{11}$$

For a given feedback rate, b, the phase space is divided into $K = 2^b$ regions. Let D_k denote the kth region corresponding to all the phase values in $[\angle w_k - \pi/K\ ,\ \angle w_k + \pi/K)$, where $\angle w_k = 2\pi k/K$ as defined in (9). If r falls within D_k, the transmitted signal should be multiplied by w_k^* in order to be rotated back towards the real axis. The receiver will then send b bits of

feedback, communicating the phase shift that has to be applied to the node's signal. Thus, the phase rotation, ϕ, that the sensor should apply to its signal will have one of the values contained in $\mathcal{S}_K$, as given in (8). The new received phase for the synchronized node will then be:

$$\tilde{\psi} \triangleq \psi + \phi \tag{12}$$

where $\phi = -\angle w_k$. At the end of the synchronization procedure, when all the N nodes have been synchronized, the final NRSS, according to (3) and (4), can be written as

$$|\hat{\mathcal{R}}_{N,K}| = \frac{1}{N}\left|\sum_{i=1}^{N} e^{j\tilde{\psi}_i}\right| \tag{13}$$

where the phases $\tilde{\psi}_i$ are the received phases after synchronization.

V. Analysis of the SDDB Algorithm

A. Noiseless Scenario

If the noise is negligible, v can be estimated exactly. For a given K, the optimum beamforming weight $\hat{w}_k$ out of the set in (9) is

$$\hat{w}_k = \arg\min_{w_k \in \mathcal{W}_K} \|v - w_k\|^2. \tag{14}$$

By using this criterion, the beamforming coefficient with minimum angular distance from v is chosen, which gives the optimal quantized phase pre-compensation to align the node to the real axis. For $K = 4$, this is graphically illustrated in Fig. 1(a), where region boundaries are marked with dashed lines. In Fig. 1(a), v falls in D_1, hence w_1 will be chosen and $\phi = -\pi/2$. Without noise, the synchronized phases $\tilde{\psi}_i$ are independent and uniform in D_0, i.e., in $[-\pi/K, +\pi/K)$. This is because the unsynchronized phases ψ_i are uniform in $[0, 2\pi)$ and the decision in (14) is noiseless, hence all the nodes will receive the correct information relative to their beamforming weight. This will then lead their synchronized phases to be uniformly distributed around the bias and to yield the best achievable RSS for a given K. The performance is limited exclusively by the resolution K, and it is therefore of interest to characterize how the NRSS behaves as a function thereof. The following result informs of that behavior.

Proposition 1: In the absence of noise, the expected value of the NRSS behaves as

$$\mathbb{E}\left[|\hat{\mathcal{R}}_{N,K}|\right] = 1 - \left(1 - \frac{1}{N} + \frac{1}{N^3}\right)\frac{\pi^2}{6K^2} + o\left(\frac{1}{K^2}\right). \tag{15}$$

Proof: See Appendix A.

Taking advantage of the fact that the number of nodes is typically large, we can further derive a lower bound on $\mathbb{E}[|\hat{\mathcal{R}}_{N,K}|]$ that is very tight for values of N of interest and exact for $N \to \infty$.

Proposition 2: In the absence of noise, the expected value of the NRSS satisfies

$$\mathbb{E}\left[|\hat{\mathcal{R}}_{N,K}|\right] \geq \mathbb{E}\left[\Re(\hat{\mathcal{R}}_{N,K})\right] \tag{16}$$

$$= \frac{K}{\pi}\sin\left(\frac{\pi}{K}\right) \tag{17}$$

where $\Re(\cdot)$ denotes real part.

Proof: See Appendix A.

Indeed, since without noise the synchronized angles are uniformly distributed around zero, the corresponding imaginary parts cancel out as $N \to \infty$.

Fig. 2 compares the NRSS obtained through Monte-Carlo simulation for increasing K, with its expansion in Proposition 1 and with the lower bound in Proposition 2. A number of 10^5 Monte-Carlo iterations has been considered to obtain the average NRSS for different values of K. As can be seen, the lower bound is very tight already for $N = 100$. Fig. 3 illustrates the tightness of the lower bound in Proposition 2 with $K = 2$, which is the worst case. Since we have shown that the tightness increases with both K and N, the bound becomes in fact exact if either of them grows without bound. The plot in Fig. 3 represents the achievable gain as a function of N_s, i.e., the number of synchronized nodes. This shows what the achievable normalized gain would be if N_s nodes were transmitting, and it is obtained by multiplying (17) by N_s/N.

Next, the second raw moment of $|\hat{\mathcal{R}}_{N,K}|$ is characterized.

Proposition 3: In the absence of noise,

$$\mathbb{E}\left[|\hat{\mathcal{R}}_{N,K}|^2\right] = \frac{1}{N} + \frac{N-1}{N}\left(\frac{K}{\pi}\right)^2 \sin^2\left(\frac{\pi}{K}\right). \tag{18}$$

Proof: See Appendix B.

Using Proposition 3, the variance of $|\hat{\mathcal{R}}_{N,K}|$ can be easily established.

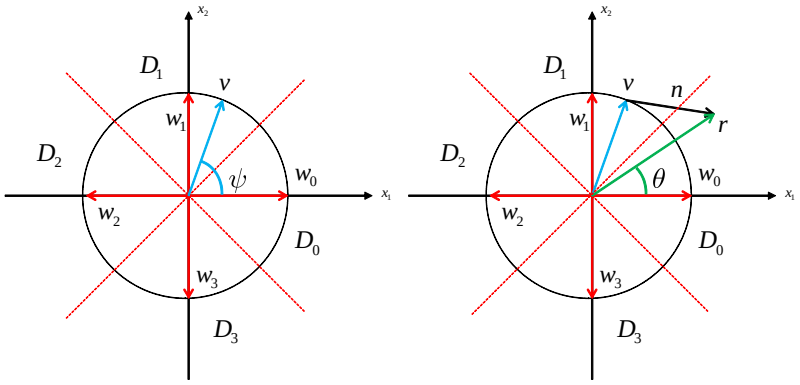

(a) $K = 4$ without noise. (b) $K = 4$ with noise.

Fig. 1. Example of phase quantization: using $\mathcal{S}_K$ is equivalent to quantizing the phase space in K regions.

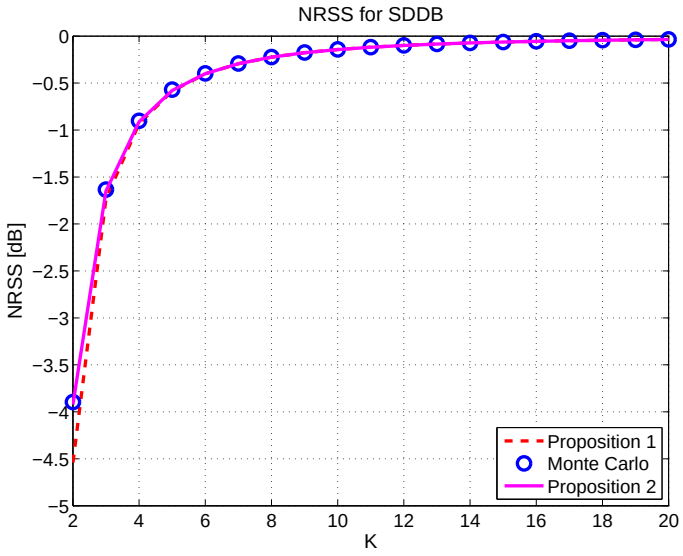

Fig. 2. Achievable NRSS with SDDB in noiseless conditions, with $N = 100$, as a function of K: Monte-Carlo simulation results compared with the analytical expressions in Propositions 1 and 2.

B. Impact of Noise

When the noise term in (11) is not negligible, the receiver will have to choose $\hat{w}_k$ based on the noisy received signal, r, as follows:

$$\hat{w}_k = \arg\min_{w_k \in \mathcal{W}_K} \|r - w_k\|^2. \tag{19}$$

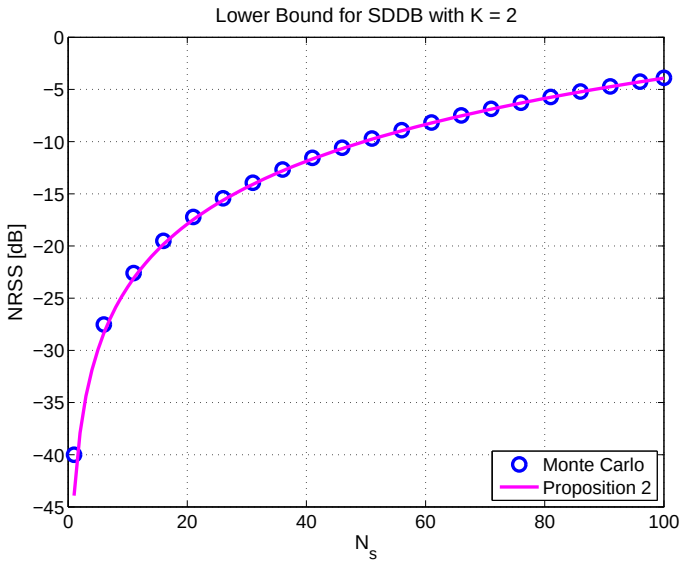

Fig. 3. Lower bound for the achievable NRSS for SDDB when $K = 2$; expression (17) is used; $N = 100$.

However, since the actual goal of the receiver is aligning v, the useful part of r, there will be a non-zero probability of making an incorrect decision. Choosing a wrong phase shift will not yield the optimum NRSS that is achievable for a given K.

1) Achievable NRSS for Finite K: Let us first investigate the effect of noise on the NRSS when K is finite, which corresponds to the practical cases of constrained capacity on the feedback link. Invoking the polar representation

$$r = Ae^{j\Theta} \tag{20}$$

the decision in (19) now depends exclusively on Θ. If Θ falls within D_k, the signal for the node in question will be multiplied by w_k^*. Clearly, this can lead to a wrong decision, as shown in Fig. 1(b). Due to the noise, therefore, the synchronized phases are no longer uniformly distributed and are not even necessarily within D_0. In this case, the distribution of the synchronized phases and, as a result, the NRSS will depend on the received SNR. We define the per-node SNR as

$$\gamma \triangleq \frac{1}{\sigma^2} \tag{21}$$

and denote the SNR-dependent normalized resultant by $\hat{\mathcal{R}}_{N,K,\gamma}$. The result that follows is a counterpart to Proposition 2, but with noise accounted for. As in the noiseless case, the bound

is tight for values of N of interest and exact for $N \to \infty$.

Proposition 4: In the presence of noise,

$$\mathbb{E}\left[|\hat{\mathcal{R}}_{N,K,\gamma}|\right] \geq \frac{K}{2\pi} \int_{-\frac{\pi}{K}}^{+\frac{\pi}{K}} \sum_{k=0}^{K-1} \cos\left(\psi' - k\frac{2\pi}{K}\right) p_{D_k|\psi=\psi'}\, d\psi' \tag{22}$$

where $p_{D_k|\psi=\psi'}$ is the probability that Θ falls within D_k conditioned to ψ being ψ', namely

$$p_{D_k|\psi=\psi'} = \text{Prob}\{\Theta \in D_k | \psi = \psi'\} = \int_{k\frac{2\pi}{K}-\frac{\pi}{K}}^{k\frac{2\pi}{K}+\frac{\pi}{K}} f_{\Theta|\psi=\psi'}(\theta) d\theta \tag{23}$$

where

$$f_{\Theta|\psi=\psi'}(\theta) = \frac{1}{2\pi} e^{-\gamma} \left\{1 + 2e^{\gamma \cos^2(\theta-\psi')} \sqrt{\gamma\pi} \cos(\theta - \psi') \left[1 - \mathcal{Q}\left(\sqrt{2\gamma} \cos(\theta - \psi')\right)\right]\right\} \tag{24}$$

with $\mathcal{Q}(\cdot)$ the Gaussian Q-function

$$\mathcal{Q}(x) \triangleq \frac{1}{\sqrt{2\pi}} \int_x^{+\infty} e^{-\frac{z^2}{2}} dz. \tag{25}$$

Proof: See Appendix C.

For $\gamma \to \infty$, the right-hand-side of (24) becomes a delta function at $\theta = \psi'$ which reduces (22) to the noiseless expression in Proposition 2 and, as mentioned at that point, the performance becomes limited only by the finite granularity K.

Particularly insightful is the analysis in the low- and high-SNR regimes. The former is representative of the conditions in which an actual sensor network necessitating of distributed beamforming might have to operate, and the latter serves as a bridge to the noiseless results presented earlier.

Proposition 5: At low SNR,

$$\mathbb{E}\left[|\hat{\mathcal{R}}_{N,K,\gamma}|\right] \geq \sqrt{\frac{\gamma}{\pi}} \frac{K}{2} \sin\left(\frac{\pi}{K}\right) + o(\gamma). \tag{26}$$

Proof: See Appendix C.

Fig. 4 exemplifies the lower bound for the achievable NRSS in the presence of noise for $K = 2$; the exact expression in (22) is represented, together with its low- and high-SNR expansions respectively (26) and (17). Fig. 5 presents the same result for $K = 4$. In both figures, the curve obtained through Monte-Carlo simulation is also represented. The average NRSS is considered

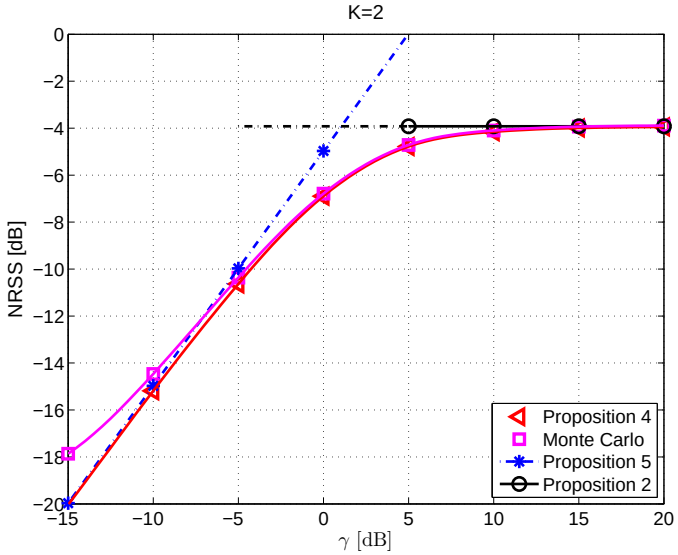

Fig. 4. Lower bound for the achievable NRSS for SDDB for $K = 2$ as a function of the SNR with its approximations for $\gamma \to 0$, shown in (26) and $\gamma \to \infty$, shown in (17); the curve obtained through simulation is also represented, with 10^5 Monte-Carlo iterations; $N = 100$.

for different values of SNR, ranging from -15 to $+20$ dB. Except for very low SNR, the bound is very tight. Fig. 6 compares the lower bound with Monte-Carlo curves (10^5 trials) obtained with different values of nodes in the network, N, more specifically for $N = 20$, 50, 100, and for $K = 2$. As can be seen, for values of SNR of relevance, such as the interval $[-5, +5]$ dB, the bound appears to be tight even for small N and small K. Clearly, the bound becomes more accurate as the number of nodes in the network increases. Fig. 7 represents angular histograms for different values of SNR, and for $K = 2$. When the SNR is low, the phases remain spread out because of the high probability with which noise prevents the receiver from reporting the correct feedback. At high SNR, in contrast, the final distribution is fairly uniform over the correct slice of the plane (for $K = 2$).

As can be appreciated, the combination of the low- and high-SNR expressions is valid over a fairly wide range of SNRs.

2) Achievable NRSS for $K \to \infty$: With infinite resolution, the regions D_k collapse to punctual real phase values. There is no constraint on the capacity of the feedback link and thus the

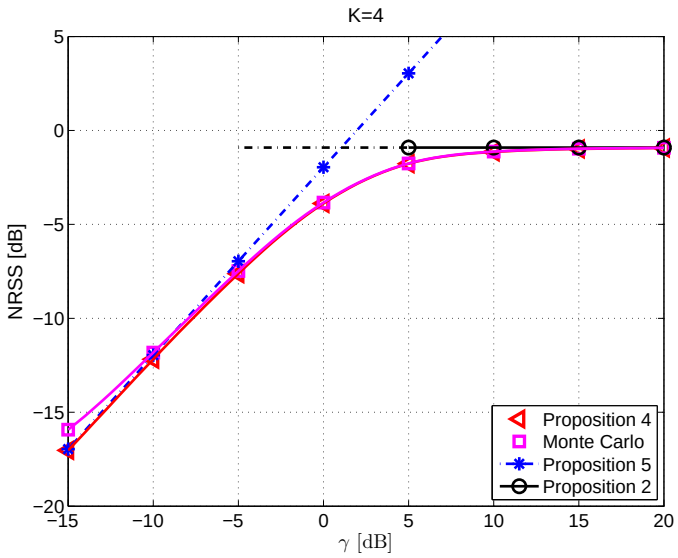

Fig. 5. Lower bound for the achievable NRSS for SDDB for $K = 4$ as a function of the SNR with its approximations for $\gamma \to 0$, shown in (26) and $\gamma \to \infty$, shown in (17); the curve obtained through simulation is also represented, with 10^5 Monte-Carlo iterations; $N = 100$.

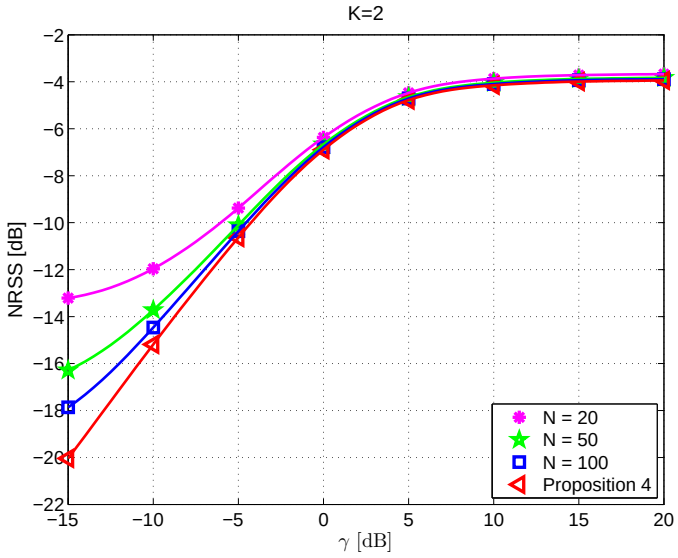

Fig. 6. Lower bound for the achievable NRSS for SDDB with $K = 2$ as a function of the SNR compared with Monte-Carlo simulations (10^5 trials) with different values of N.

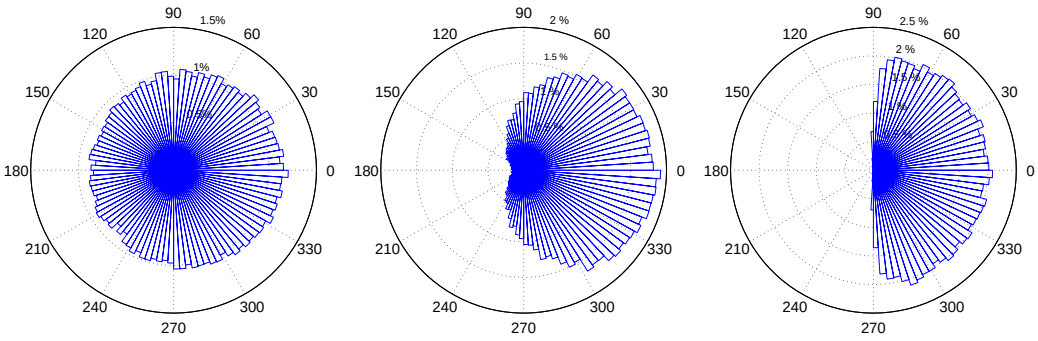

(a) SNR $= -20$ dB (b) SNR $= 0$ dB (c) SNR $= +20$ dB

Fig. 7. Angular histograms for SDDB with resolution $K = 2$ for different SNR values.

performance is limited exclusively by noise. As it turns out, this limiting behavior is approached closely with modest values of K, which reinforces the value of the resulting expressions.

Proposition 6: The expected value of $|\hat{\mathcal{R}}_{N,\infty,\gamma}|$ satisfies

$$\mathbb{E}\left[|\hat{\mathcal{R}}_{N,\infty,\gamma}|\right] \geq \frac{e^{-\gamma/2}}{2}\sqrt{\pi\gamma}\left(I_0\left(\frac{\gamma}{2}\right) + I_1\left(\frac{\gamma}{2}\right)\right) \tag{27}$$

where $I_0(\cdot)$ and $I_1(\cdot)$ are the modified Bessel functions of first kind of orders 0 and 1, respectively.

Proof: See Appendix D.

The low- and high-SNR behaviors with noise and infinite resolution are obtained by expanding Proposition 6. At low SNR, the right-hand side of (27) behaves as

$$\frac{\sqrt{\pi\gamma}}{2} + o\left(\gamma\right) \tag{28}$$

while, at high SNR, it behaves as

$$1 + \left(1 + e^{-\gamma}\right) O\left(\frac{1}{\gamma}\right). \tag{29}$$

Fig. 8 compares (27), (28), (29), and the curve obtained through Monte-Carlo simulation. The lower bound for the achievable NRSS is plotted as a function of the SNR. It can be seen that (28) closely matches (27) below roughly -5 dB while (29) closely matches it above roughly 5 dB.

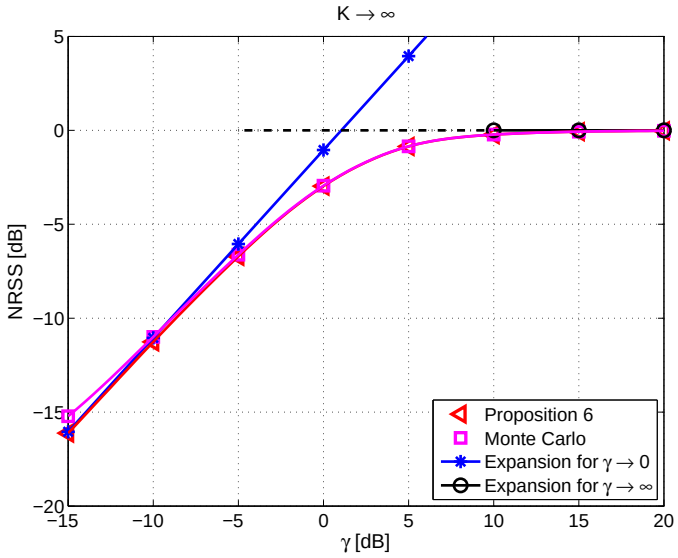

Fig. 8. Achievable NRSS for SDDB when $K \to \infty$ as a function of the SNR expressed in (27), and its approximations for $\gamma \to 0$, expressed in (28), and $\gamma \to \infty$, expressed in (29); the curve obtained through simulation is also represented, with 10^5 Monte-Carlo iterations; $N = 100$.

VI. Performance Comparison: Random v. Deterministic

In this section, we compare the R1BF and the SDDB approaches both without and with noise. The curves again are the result of Monte-Carlo simulation campaigns with 10^5 iterations. A network of $N = 100$ nodes is considered, and the initial phases prior to synchronization are modeled as uniform in $[0, 2\pi)$.

A. Noiseless Scenario

In Fig. 9, the noiseless performance of the random algorithm (R1BF, cf. Section III), is illustrated in terms of the NRSS improvement over time. A window of 450 time slots is considered. The distribution for the random shifts $f_{\delta_i}(\cdot)$ is uniform in $[-\pi/\beta, +\pi/\beta]$ for every i, and the curves for distinct values of β are shown. As can be seen, a larger variance allows for a very rapid NRSS increase in the initial stages, but at the price of a slow eventual convergence. In contrast, smaller variances yield a very low initial growth rate, in return for faster convergence as the NRSS approaches its maximum. Authors in [1] show how an adaptive behavior improves

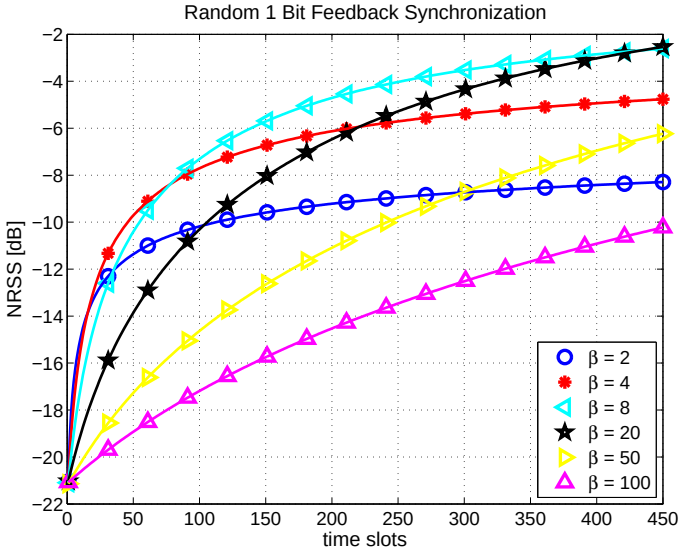

Fig. 9. NRSS for R1BF without noise, with $N = 100$, and $f_{\delta_i}(\cdot)$ uniform in $[-\pi/\beta, +\pi/\beta]$ for every i.

convergence. In this case, nodes can adjust the variance of the distribution, optimizing it at each iteration according to the NRSS value. But this approach is practically unfeasible since it would require the nodes to have full knowledge of the NRSS at each step, and thus the receiver to send a much higher-rate feedback. By considering the variance of this distribution to be fixed, we relate to a more practical and realistic case.

Fig. 10 is related to SDDB without noise (cf. Section V-A), presenting the NRSS as a function of the number of activated and synchronized devices, $N_{\text{s}}[m]$, as given in (4). The plot can also be interpreted as a function of time, since nodes are synchronized successively (one per time slot) and thus the curves indicate the NRSS that would be attained by the activated nodes after a certain number of rounds. The first value of each curve corresponds to a single-node transmission, and the last value ($N_{\text{s}}[m] = N$) is the NRSS achieved when the complete network is beamforming. The different curves correspond to different resolutions, K. When the receiver can only send one bit of feedback ($K = 2$), the achievable NRSS is 4 dB away from the maximum achievable value. When $K = 4$, the attainable NRSS is within 1 dB of the maximum. As K increases even further, the improvement becomes minute. Hence, the most relevant cases are (*i*) $K = 2$, when the feedback rate is 1 bit and a fair comparison with R1BF is possible, (*ii*) $K = 4$, which shows

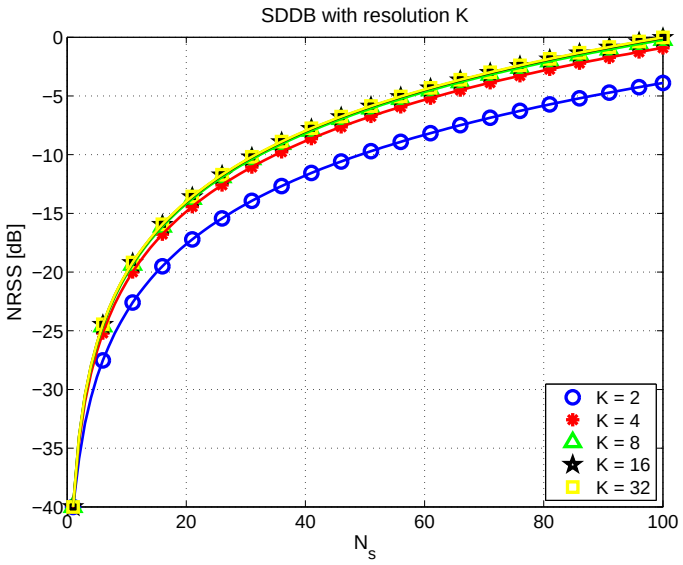

Fig. 10. NRSS for SDDB without noise, with parameter K; $N = 100$.

that by simply adding one more feedback bit, SDDB yields very high gains after only N time rounds, and (*iii*) $K \to \infty$, which approximates well all the remaining values of K.

Fig. 11 presents a noiseless comparison between R1BF and SDDB. The graph depicts the NRSS as a function of time (for SDDB, recall, the NRSS at a given time slot m indicates the NRSS achieved by m synchronized nodes). The R1BF curves correspond to different values of β, and the curves for SDDB represent the cases $K = 2$ and $K = 4$. During the first time slot, all the unsynchronized nodes in R1BF yield an initial normalized gain of $1/\sqrt{N}$. For SDDB, in turn, the initial gain corresponds to a single-node transmission. With one bit of feedback, SDDB starts outperforming R1BF after 50 time slots and it becomes roughly 4 dB better after 100 slots. This comparison is for $\beta = 4$, which is the best choice for R1BF in this time frame. This improvement comes with an increase of network coordination with respect to R1BF. Nodes in fact have to be indexed and they must transmit in a predefined order. Indexing can be done once, when the network is deployed. Transmitting in turn can be achieved with a token passing mechanism, or the feedback itself could trigger the progressive awakening of each sensor. At the price of an extra feedback bit, SDDB starts outperforming R1BF after only 30 time slots, becoming roughly

8 dB better after 100 time slots. In addition, recall, SDDB has an N-fold power saving factor per time slot. A time frame of an order of magnitude larger is required for R1BF to achieve gains comparable to the ones achieved by SDDB in 100 time slots. As mentioned in Section II, in practical scenarios the phase of each local oscillator drifts over time, causing progressive carrier misalignment and consequent loss in terms of beamforming gain. Both oscillator dynamics and frequency mismatches due to imperfect carrier synchronization have to be taken into account and properly modeled to identify the time interval within which quasi-static oscillators' phase can be assumed, identified as Oscillators' Coherence Time (OCT). The OCT interval then determines the rate of periodic phase re-synchronization in order to maintain tracking, according to the level of tolerance of the application. The problem of modeling phase drift has been studied, for example, in [36] and [11]. In both these works, the drift is modeled as a non-stationary Gaussian process with zero mean and a time-dependent variance. For instance, in [11] the time-dependent variance of the drift $\sigma_{\mathrm{d}}^2(t)$ is expressed as $\sigma_{\mathrm{d}}^2(t) = c\Delta t$, where c is a parameter dependent on the physical properties of the local oscillator and is measured in rad$^2 \times$ Hz, and Δt is the considered time frame in seconds. This model is based on the work in [37]. As stated in [11], for low-cost radio-frequency oscillators, parameter c ranges from 1 to 20 rad$^2 \times$ Hz. Taking $c = 10$ as the typical drift parameter, for a network of $N = 100$ nodes, it can be verified that the beamforming gain experiences a 5 dB decrease with respect to the value achieved after phase synchronization, in a time frame of 100 ms. Clearly signals continue experiencing misalignment during the synchronization procedure itself, hence, reduction of convergence time is mandatory, and this is exactly the issue we address in this work. Moreover, when phase drift is severe, or when the size of the network is so large that carrier synchronization requires long time spans, adaptive tracking methods can be employed, such as the ones suggested in [21], [22], which have been proven to be very robust against channel drift. Since the statistics of the phase drift are known, ad hoc phase re-alignment routines can be tailored to the application requirements. These are all very interesting points that pave the way for future developments of this work.

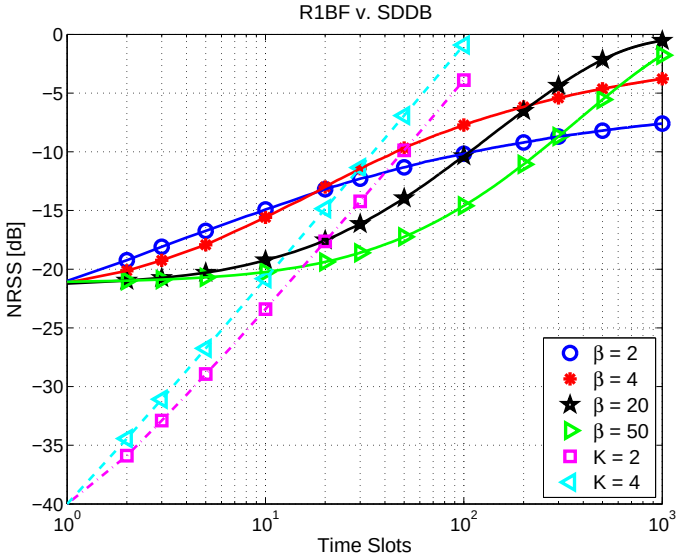

Fig. 11. Noiseless comparison between R1BF and SDDB, with different shift distributions for R1BF ($f_{\delta_i}(\cdot)$ uniform in $[-\pi/\beta, +\pi/\beta]$ for every i), and $K = 2,\ 4$ for SDDB; $N = 100$.

B. Noisy Scenario

Fig. 12 represents a comparison (through simulation) between the R1BF and SDDB schemes when the SNR is low, specifically 0 dB, which corresponds to $\sigma^2 = 1$, in a time frame of 10^3 time slots. As in the noiseless case, SDDB outperforms R1BF, although the gap between them is somewhat smaller. Still, in order for R1BF to achieve a gain comparable to what SDDB achieves in 100 time slots, a time frame of an order of magnitude longer is required. The R1BF curves are for $\beta = 4$, 10, 20, respectively, whereas the SDDB curves are for $K = 2$ and $K = 4$. After 80 slots, SDDB with one feedback bit starts outperforming R1BF with $\beta = 4$, which is the best performing one, and the gap after 100 time slots is roughly 2 dB. With two bits of feedback, the crossover occurs after less than 50 slots and the gap after 100 time slots increases to roughly 5 dB.

VII. Conclusion

We have presented a new phase-alignment algorithm for distributed beamforming. This algorithm can be regarded as a member of the family of deterministic algorithms initiated in

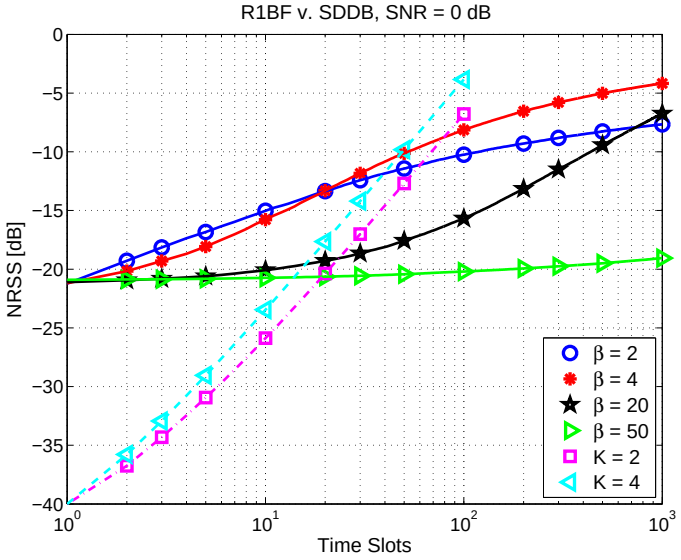

Fig. 12. Simulated comparison between R1BF and SDDB in the presence of noise; $f_{\delta_i}(\cdot)$ uniform in $[-\pi/\beta, +\pi/\beta]$ for every i; $N = 100$.

[21]. Based, as previous deterministic algorithms, on a closed-loop procedure involving feedback from the receiver, its main novelty lies in its sequential nature: each node transmits only once throughout the entire alignment process and hence the power consumption scales with N. This drastically reduces the power consumption with respect to all existing solutions (deterministic and random), where each node must transmit repeatedly throughout the process, thereby scaling the power consumption with N^2. This advantage might be crucial for boosting the life span of a sensor network.

In contrast with most previous analyses of distributed beamforming, in this paper noise has been brought explicitly into the models. Analytic expressions that characterize the performance of the new algorithm, without and with noise, have been put forth, with emphasis on various limiting regimes of interest.

The performance of the new algorithm has been compared against those of the schemes hitherto formulated, and it has been shown to converge faster than random algorithms with identical feedback rate and as fast as all other deterministic algorithms. In both cases, recall, this is achieved with drastically less power consumption.

APPENDIX A
PROOF OF PROPOSITIONS 1 AND 2

For notational compactness, let us define

$$x \triangleq \frac{1}{N}\sum_{i=1}^{N}\cos\tilde{\psi}_i \tag{30}$$

$$y \triangleq \frac{1}{N}\sum_{i=1}^{N}\sin\tilde{\psi}_i \tag{31}$$

where $\tilde{\psi}_1,\ldots,\tilde{\psi}_N$ are independent and identically distributed uniformly in $[-\pi/K,+\pi/K)$ and the NRSS is simply $\sqrt{x^2+y^2}$. For $K\to\infty$, clearly $x\to 1$ and $y\to 0$. Thus, we expand the NRSS around $x=1$ and $y=0$ obtaining

$$\sqrt{x^2+y^2} = x + \frac{3}{2}y^2 - \frac{3}{2}xy^2 + \frac{1}{2}x^2y^2 + O\left((x-1)^3\right) + O\left((x-1)^3\right)y^2 + O\left(y^3\right). \tag{32}$$

We now take expectations over $\tilde{\psi}_1,\ldots,\tilde{\psi}_N$. For the first term in (32),

$$\mathbb{E}\left[x\right] = \int_{-\frac{\pi}{K}}^{+\frac{\pi}{K}}\cdots\int_{-\frac{\pi}{K}}^{+\frac{\pi}{K}}\left(\frac{1}{N}\sum_{i=1}^{N}\cos\xi_i\right) f_{\tilde{\psi}_1\cdots\tilde{\psi}_N}(\xi_1,\ldots,\xi_N)d\xi_1\cdots d\xi_N \tag{33}$$

$$= \frac{1}{N}\left(\frac{K}{2\pi}\right)^N\int_{-\frac{\pi}{K}}^{+\frac{\pi}{K}}\cdots\int_{-\frac{\pi}{K}}^{+\frac{\pi}{K}}\left(\sum_{i=1}^{N}\cos\xi_i\right)d\xi_1\cdots d\xi_N \tag{34}$$

$$= \frac{K}{\pi}\sin\left(\frac{\pi}{K}\right) \tag{35}$$

$$= 1 - \frac{\pi^2}{6K^2} + o\left(\frac{1}{K^2}\right). \tag{36}$$

For the second term, in turn,

$$\mathbb{E}\left[y^2\right] = \int_{-\frac{\pi}{K}}^{+\frac{\pi}{K}}\cdots\int_{-\frac{\pi}{K}}^{+\frac{\pi}{K}}\left(\frac{1}{N}\sum_{i=1}^{N}\sin\xi_i\right)^2 f_{\tilde{\psi}_1\cdots\tilde{\psi}_N}(\xi_1,\ldots,\xi_N)d\xi_1\cdots d\xi_N \tag{37}$$

$$= \frac{1}{N^2}\left(\frac{K}{2\pi}\right)^N\int_{-\frac{\pi}{K}}^{+\frac{\pi}{K}}\cdots\int_{-\frac{\pi}{K}}^{+\frac{\pi}{K}}\left(\sum_{i=1}^{N}\sin\xi_i\right)^2 d\xi_1\cdots d\xi_N \tag{38}$$

$$= \frac{K}{2\pi N}\left(\frac{\pi}{K} - \frac{1}{2}\sin\left(\frac{2\pi}{K}\right)\right) \tag{39}$$

$$= \frac{\pi^2}{3NK^2} + o\left(\frac{1}{K^2}\right) \tag{40}$$

and, for the third term,

$$\mathbb{E}\left[xy^2\right] = \int_{-\frac{\pi}{K}}^{+\frac{\pi}{K}} \cdots \int_{-\frac{\pi}{K}}^{+\frac{\pi}{K}} \left(\frac{1}{N}\sum_{i=1}^{N}\cos\xi_i\right)\left(\frac{1}{N}\sum_{i=1}^{N}\sin\xi_i\right)^2 f_{\tilde{\psi}_1\cdots\tilde{\psi}_N}(\xi_1,\ldots,\xi_N)d\xi_1\cdots d\xi_N \quad (41)$$

$$= \frac{1}{N^3}\left(\frac{K}{2\pi}\right)^N \int_{-\frac{\pi}{K}}^{+\frac{\pi}{K}} \cdots \int_{-\frac{\pi}{K}}^{+\frac{\pi}{K}} \left(\sum_{i=1}^{N}\cos\xi_i\right)\left(\sum_{i=1}^{N}\sin\xi_i\right)^2 d\xi_1\cdots d\xi_N \quad (42)$$

$$= \frac{K}{3\pi N^2}\sin^3\left(\frac{\pi}{K}\right) + \frac{N-1}{N^2}\frac{K^2}{2\pi^2}\sin\left(\frac{\pi}{K}\right)\left(\frac{\pi}{K} - \frac{1}{2}\sin\left(\frac{2\pi}{K}\right)\right) \quad (43)$$

$$= \frac{\pi^2}{3N^2K^2} + \frac{N-1}{N^2}\frac{\pi^2}{3K^2} + o\left(\frac{1}{K^2}\right) \quad (44)$$

Finally, the fourth term in (32)

$$\mathbb{E}\left[x^2y^2\right] = \int_{-\frac{\pi}{K}}^{+\frac{\pi}{K}} \cdots \int_{-\frac{\pi}{K}}^{+\frac{\pi}{K}} \left(\frac{1}{N}\sum_{i=1}^{N}\cos\xi_i\right)^2\left(\frac{1}{N}\sum_{i=1}^{N}\sin\xi_i\right)^2 f_{\tilde{\psi}_1\cdots\tilde{\psi}_N}(\xi_1,\ldots,\xi_N)d\xi_1\cdots d\xi_N \quad (45)$$

$$= \frac{1}{N^4}\left(\frac{K}{2\pi}\right)^N \int_{-\frac{\pi}{K}}^{+\frac{\pi}{K}} \cdots \int_{-\frac{\pi}{K}}^{+\frac{\pi}{K}} \left(\sum_{i=1}^{N}\cos\xi_i\right)^2\left(\sum_{i=1}^{N}\sin\xi_i\right)^2 d\xi_1\cdots d\xi_N \quad (46)$$

$$= \frac{K}{32\pi N^3}\left(\frac{4\pi}{K} - \sin\left(\frac{4\pi}{K}\right)\right) + \frac{N-1}{N^3}\frac{K^2}{4\pi^2}\left(\frac{\pi^2}{K^2} - \frac{1}{4}\sin^2\left(\frac{2\pi}{K}\right)\right)$$

$$+ \frac{4}{3}\frac{N-1}{N^3}\left(\frac{K}{2\pi}\right)^2\sin^4\left(\frac{\pi}{K}\right)$$

$$+ 2\frac{(N-1)(N-2)}{N^3}\left(\frac{K}{2\pi}\right)^3 4\sin^2\left(\frac{\pi}{K}\right)\left(\frac{\pi}{K} - \frac{1}{2}\sin\left(\frac{2\pi}{K}\right)\right) \quad (47)$$

$$= \frac{\pi^2}{3K^2N^3} + \frac{N-1}{N^3}\frac{\pi^2}{3K^2} + \frac{N-1}{N^3}\frac{\pi^2}{3K^2} + 2\frac{(N-1)(N-2)}{N^3}\frac{\pi^2}{3K^2} + o\left(\frac{1}{K^2}\right) \quad (48)$$

By putting together (36), (40), (44), and (48), the expectation of (32) gives (15). This proves Proposition 1.

Proposition 2 follows from neglecting the imaginary part of $\hat{\mathcal{R}}_{N,K}$, in which case $\mathbb{E}[|\hat{\mathcal{R}}_{N,K}|]$ is given directly by (35).

APPENDIX B
PROOF OF PROPOSITION 3

The second raw moment of $|\hat{\mathcal{R}}_{N,K}|$ equals

$$\mathbb{E}\left[|\hat{\mathcal{R}}_{N,K}|^2\right] = \int_{-\frac{\pi}{K}}^{+\frac{\pi}{K}} \cdots \int_{-\frac{\pi}{K}}^{+\frac{\pi}{K}} \left(\frac{1}{N}\sum_{i=1}^{N}\cos\xi_i\right)^2 f_{\tilde{\psi}_1\cdots\tilde{\psi}_N}(\xi_1,\ldots,\xi_N)d\xi_1\cdots d\xi_N + \int_{-\frac{\pi}{K}}^{+\frac{\pi}{K}} \cdots \int_{-\frac{\pi}{K}}^{+\frac{\pi}{K}} \left(\frac{1}{N}\sum_{i=1}^{N}\sin\xi_i\right)^2 f_{\tilde{\psi}_1\cdots\tilde{\psi}_N}(\xi_1,\ldots,\xi_N)d\xi_1\cdots d\xi_N \tag{49}$$

$$= \frac{1}{N^2}\left(\frac{K}{2\pi}\right)^N \int_{-\frac{\pi}{K}}^{+\frac{\pi}{K}} \cdots \int_{-\frac{\pi}{K}}^{+\frac{\pi}{K}} \left(\sum_{i=1}^{N}\cos\xi_i\right)^2 d\xi_1\cdots d\xi_N + \frac{1}{N^2}\left(\frac{K}{2\pi}\right)^N \int_{-\frac{\pi}{K}}^{+\frac{\pi}{K}} \cdots \int_{-\frac{\pi}{K}}^{+\frac{\pi}{K}} \left(\sum_{i=1}^{N}\sin\xi_i\right)^2 d\xi_1\cdots d\xi_N. \tag{50}$$

The first term in (50) yields

$$\frac{K}{4\pi N}\sin\left(\frac{2\pi}{K}\right) + \frac{1}{2N} + \left(\frac{K}{\pi}\right)^2 \frac{N-1}{N}\sin^2\left(\frac{\pi}{K}\right) \tag{51}$$

whereas the second term in (50) was already evaluated in Appendix A, Eq. (39). The result equals the claim of Proposition 3.

APPENDIX C
PROOF OF PROPOSITIONS 4 AND 5

Let us lower bound $\mathbb{E}[|\hat{\mathcal{R}}_{N,K,\gamma}|]$ with $\mathbb{E}[\Re(\hat{\mathcal{R}}_{N,K,\gamma})]$ by first finding the distribution of Θ. The received complex signal r in (11) can be written as

$$r = \cos\psi + n_{\Re} + j(\sin\psi + n_{\Im}) \tag{52}$$

where, if z is a complex scalar, $z_{\Re}$ and $z_{\Im}$ represent its real and imaginary part, respectively. For a given $\psi = \psi'$, $r_{\Re}$ and $r_{\Im}$ are independent Gaussian random variables with variance $\sigma^2/2$ and mean $\cos\psi'$ and $\sin\psi'$, respectively. The PDF of r conditioned on $\psi = \psi'$ is

$$f_{r|\psi=\psi'}(\rho) = \frac{\gamma}{\pi}e^{-\gamma((\rho_{\Re}-\cos\psi')^2+(\rho_{\Im}-\sin\psi')^2)}. \tag{53}$$

Based on (53), the joint PDF of A and Θ, conditioned on $\psi = \psi'$, is then [38]

$$f_{A,\Theta|\psi=\psi'}(a,\theta) = \frac{\gamma}{\pi} a e^{-\gamma(a^2+1-2a\cos(\theta-\psi'))} \tag{54}$$

and, integrating over a, we obtain the marginal PDF of Θ conditioned on $\psi = \psi'$ as

$$f_{\Theta|\psi=\psi'}(\theta) = \int_0^{+\infty} f_{A,\Theta|\psi=\psi'}(a,\theta)da \tag{55}$$

$$= \frac{\gamma}{\pi} e^{-\gamma\sin^2(\theta-\psi')} \int_0^{+\infty} a e^{-\gamma(a-\cos(\theta-\psi'))^2} da. \tag{56}$$

The integration in (56) gives (24). The result in (22) represents $\mathbb{E}[\Re(\hat{\mathcal{R}}_{N,K,\gamma})]$ because of the following: for a given ψ', depending on the noise realization, the received signal may fall in any of the K different regions. If Θ falls within D_k, a phase shift of $2\pi k/K$ will be applied to the signal, and the phase of its useful part will be $\psi' - 2\pi k/K$. Hence, the useful part of each node's signal becomes a weighted sum of K cosines, whose phases are $\psi' - 2\pi k/K$, for $k = 0, \ldots, K-1$, and whose weights correspond to the probability of Θ being in the corresponding decision region D_k. The expression is then averaged according to the distribution of ψ that we consider uniform in $[-\pi/K, +\pi/K)$. Due to the symmetry of the system, this is equivalent to considering ψ uniformly distributed in any of the K regions. Proposition 4 is thus proven.

For low SNR, (24) expands as

$$f_{\Theta,\gamma|\psi=\psi'}(\theta) = \frac{1}{2\pi} + \sqrt{\gamma}\frac{\cos(\theta-\psi')}{2\sqrt{\pi}} + \gamma\frac{(2\cos^2(\theta-\psi')-1)}{2\pi} + o(\gamma) \tag{57}$$

and, plugging (57) into (23), we obtain

$$p_{D_k,\gamma|\psi=\psi'} = \frac{1}{K} + \sqrt{\frac{\gamma}{\pi}}\sin\left(\frac{\pi}{K}\right)\cos\left(\psi' - \frac{k2\pi}{K}\right) + \frac{\gamma}{2\pi}\sin\left(\frac{2\pi}{K}\right)\cos\left(2\psi' - \frac{k4\pi}{K}\right) + o(\gamma). \tag{58}$$

By using (58) in (22), we obtain:

$$\mathbb{E}\left[|\hat{\mathcal{R}}_{N,K,\gamma}|\right] \geq \frac{1}{\pi}\sin\left(\frac{\pi}{K}\right)\sum_{k=0}^{K-1}\cos\left(\frac{2k\pi}{K}\right) + \sqrt{\frac{\gamma}{\pi}}\frac{K}{8\pi}\sin\left(\frac{\pi}{K}\right)\left[4\pi + 2\sin\left(\frac{2\pi}{K}\right)\right.$$
$$\left.\cdot\sum_{k=0}^{K-1}\cos\left(\frac{4k\pi}{K}\right)\right] + \gamma\frac{K}{12\pi^2}\sin\left(\frac{2\pi}{K}\right)\sum_{k=0}^{K-1}\cos\left(\frac{2k\pi}{K}\right)\left[3\sin\left(\frac{\pi}{K}\right)\right.$$
$$\left.+\sin\left(\frac{3\pi}{K}\right)\left(2\cos\left(\frac{4k\pi}{K}\right)-1\right)\right] + o(\gamma). \tag{59}$$

Expression (59) can be simplified by observing that, for every K

$$\sum_{k=0}^{K-1}\cos\left(\frac{2\pi k}{K}\right) = \frac{1}{2}\sum_{k=0}^{K-1}\left(e^{j\frac{2\pi k}{K}} + e^{-j\frac{2\pi k}{K}}\right)$$
$$= \frac{1}{2}\left(\frac{1-e^{j2\pi}}{1-e^{j\frac{2\pi}{K}}} + \frac{1-e^{-j2\pi}}{1-e^{-j\frac{2\pi}{K}}}\right)$$
$$= 0. \tag{60}$$

This is also valid for the summation of $\cos(4k\pi/K)$ terms in (59). Hence, the coefficients that multiply the terms of orders 0 and 1 in the expression (59) are always zero, and this simplification yields (26). This proves Proposition 5.

APPENDIX D
PROOF OF PROPOSITION 6

Without loss of generality, we can fix $\psi = 0$, which is equivalent to fixing any other value in $[0, 2\pi)$. With that $r = 1 + n$ and (53) becomes

$$f_{r|\psi=0}(\rho) = \frac{\gamma}{\pi}e^{-\gamma((\rho_{\Re}-1)^2+\rho_{\Im}^2)}, \tag{61}$$

from which $f_{A,\Theta|\psi=0}(a,\theta)$ in turn becomes

$$f_{A,\Theta|\psi=0}(a,\theta) = \frac{a}{\pi}\gamma e^{-\gamma(a^2+1-2a\cos\theta)} \tag{62}$$

and the distribution of Θ conditioned on $\psi = 0$ is given by

$$f_{\Theta|\psi=0}(\theta) = \int_0^{+\infty} f_{A,\Theta}(a,\theta)da \tag{63}$$

$$= \frac{\gamma}{\pi} e^{-\gamma \sin^2\theta} \int_0^{+\infty} a e^{-\gamma(a-\cos\theta)^2} da. \tag{64}$$

The integration in (64) gives

$$f_{\Theta|\psi=0}(\theta) = \frac{1}{2\pi} e^{-\gamma} \left\{ 1 + 2e^{\gamma\cos^2\theta} \sqrt{\pi\gamma}\cos\theta \left[1 - \mathcal{Q}\left(\sqrt{2\gamma}\cos\theta \right) \right] \right\}. \tag{65}$$

In order to de-condition (65), the following integration can be carried out:

$$\int_{-\pi}^{+\pi} f_\Theta(\theta - \psi')\delta(\psi')d\psi' = f_\Theta(\theta) \tag{66}$$

because ψ is conditioned to having a punctual deterministic value, and hence its distribution is a delta function.

The first raw moment of the real part of $\hat{\mathcal{R}}_{N,\infty,\gamma}$ can be written as

$$\mathbb{E}\left[\Re\left(\hat{\mathcal{R}}_{N,\infty,\gamma} \right) \right] = \int_{-\pi}^{+\pi} \cos\theta f_\Theta(\theta) d\theta. \tag{67}$$

This derives from the fact that the node will rotate its vector exactly by θ, which is the phase observed at the receiver. As a consequence, instead of remaining on the real axis, as it would if the feedback were correct, its phase is centered on zero with distribution $f_\Theta(\cdot)$. In order to integrate (67), we proceed as follows: reordering the terms in (65), we write

$$f_\Theta(\theta) = \frac{1}{2\pi} e^{-\gamma} + \sqrt{\frac{\gamma}{4\pi}} e^{-\gamma\sin^2\theta}\cos\theta + \sqrt{\frac{\gamma}{4\pi}} \left(1 - 2\mathcal{Q}(\sqrt{2\gamma}\cos\theta) \right) e^{-\gamma\sin^2\theta}\cos\theta \tag{68}$$

and we then define the integrals

$$\mathcal{I}_1 \triangleq \frac{1}{2\pi} e^{-\gamma} \int_{-\pi}^{+\pi} \cos\theta d\theta \tag{69}$$

$$\mathcal{I}_2 \triangleq \sqrt{\frac{\gamma}{4\pi}} \int_{-\pi}^{+\pi} e^{-\gamma\sin^2\theta}\cos^2\theta d\theta \tag{70}$$

$$\mathcal{I}_3 \triangleq \sqrt{\frac{\gamma}{4\pi}} \int_{-\pi}^{+\pi} \left(1 - 2\mathcal{Q}(\sqrt{2\gamma}\cos\theta) \right) e^{-\gamma\sin^2\theta}\cos^2\theta d\theta \tag{71}$$

such that (67) is simply $\mathcal{I}_1 + \mathcal{I}_2 + \mathcal{I}_3$. Obviously, (69) is zero and (71) is also zero because the integrand is an odd function for $\theta \in [-\pi, +\pi)$. In turn, (27) admits the closed form that constitutes the claim of Proposition 6.

REFERENCES

[1] R. Mudumbai, J. Hespanha, U. Madhow, and G. Barriac, "Distributed transmit beamforming using feedback control," *IEEE Trans. on Inf. Theory*, vol. 56, no. 1, pp. 411–26, Jan. 2010.

[2] R. Mudumbai, B. Wild, U. Madhow, and K. Ramchandran, "Distributed beamforming using 1 bit feedback: From concept to realization," in *Proc. 44th Annu. Allerton Conf. Commun., Control and Computing*, Monticello, IL, Sep. 2006, pp. 1020–7.

[3] R. Mudumbai, J. Hespanha, U. Madhow, and G. Barriac, "Scalable feedback control for distributed beamforming in sensor networks," in *Proc. IEEE Int. Symp. on Inf. Theory (ISIT'05)*, Adelaide, Australia, Sep. 2005, pp. 137–41.

[4] G. Barriac, R. Mudumbai, and U. Madhow, "Distributed beamforming for information transfer in sensor networks," in *Proc. 3rd Int. Symp. Inf. Processing in Sensor Netw. (IPSN'04)*, Berkeley, CA, Apr. 2004, pp. 81–8.

[5] C. Lin, V. V. Veeravalli, and S. P. Meyn, "A random search framework for convergence analysis of distributed beamforming with feedback," *IEEE Trans. on Inf. Theory*, vol. 56, no. 12, pp. 6133–41, Dec. 2010.

[6] S. Song, J. S. Thompson, P. J. Chung, and P. M. Grant, "Improving the one-bit feedback algorithm for distributed beamforming," in *Proc. Wireless Comm. and Networking Conf. (WCNC'10)*, Sydney, Australia, Apr. 2010, pp. 1–6.

[7] J. A. Bucklew and W. A. Sethares, "Convergence of a class of decentralized beamforming algorithms," *IEEE Trans. on Sig. Pro.*, vol. 56, no. 6, pp. 2280–88, Jun. 2008.

[8] C. S. Tseng, C. C. Chen, and C. Lin, "A bio-inspired robust adaptive random search algorithm for distributed beamforming," in *Proc. IEEE Int. Conf. on Communications (ICC'11)*, Kyoto, Japan, Jun. 2011, pp. 1–6.

[9] J. Thukral and H. Bölcskei, "Distributed spatial multiplexing with 1-bit feedback," in *Proc. 45th Annu. Allerton Conf. Commun., Control and Computing*, Monticello, IL, Sep. 2007, pp. 502–9.

[10] P. Jeevan, S. Pollin, A. Bahai, and P. P. Varaiya, "Pairwise algorithm for distributed transmit beamforming," in *Proc. IEEE Int. Conf. on Communications (ICC'08)*, Beijing, China, May 2008, pp. 4245–9.

[11] D. R. Brown and H. V. Poor, "Time-slotted round trip carrier synchronization for distributed beamforming," *IEEE Trans. on Sig. Pro.*, vol. 56, no. 11, pp. 5630–43, Nov. 2008.

[12] I. Ozil and D. R. Brown, "Time-slotted round-trip carrier synchronization," in *Proc. 41st Asilomar Conf. Signals, Sys., Comp.*, Pacific Grove, CA, Nov. 2007, pp. 1781–5.

[13] A. Bletsas, A. Lippman, and J. N. Sahalos, "Simple, zero-feedback, distributed beamforming with unsynchronized carriers," *IEEE Journal on Selected Areas in Comm.*, vol. 28, no. 7, pp. 1046–54, Sep. 2010.

[14] P. Fertl, A. Hottinen, and G. Matz, "Perturbation-based distributed beamforming for wireless relay networks," in *Proc. IEEE Global Telecom. Conf. (GLOBECOM'08)*, New Orleans, LA, Nov. 2008, pp. 1–5.

[15] M. Johnson, M. Mitzenmacher, and K. Ramchandran, "Distributed beamforming with binary signaling," in *Proc. IEEE Int. Symp. on Inf. Theory (ISIT'08)*, Toronto, Canada, Jul. 2008, pp. 890–4.

[16] D. R. Brown, G. Prince, and J. McNeill, "A method for carrier frequency and phase synchronization of two autonomous cooperative transmitters," in *Proc. IEEE 6th Workshop on Signal Processing Adv. Wireless Commun.*, New York, NY, Jun. 2005, pp. 260–4.

[17] Y.-S. Tu and G. Pottie, "Coherent cooperative transmission from multiple adjacent antennas to a distant stationary antenna through AWGN channels," in *Proc. IEEE 55th Vehicular Tech. Conf., (VTC Spring '02)*, vol. 1, Birmingham, AL, May 2002, pp. 130–4.

[18] W. Haijie, Y. Ding, and H. M. Kwon, "Phase synchronization for distributed sensor networks in feedback bit errors," in *Proc. IEEE Int. Conf. on Wireless Comm., Networking and Information Security (WCNIS)'10*, Beijing, China, Jun. 2010, pp. 282–6.

[19] W. Tushar, D. Smith, A. Zhang, T. Lamahewa, and T. Abhayapala, "Distributed transmit beamforming: Phase convergence improvement using enhanced one-bit feedback," in *Proc. IEEE Wireless Comm. and Networking Conference (WCNC)'12*, Paris, France, Apr. 2012, pp. 528–32.

[20] G. Lim and L. J. Cimini, "Partitioned one-bit feedback for cooperative beamforming," in *Proc. 44th Annual Conf. on Information Sciences and Syst. (CISS)'10*, Princeton, NJ, Mar. 2010, pp. 1–5.

[21] I. Thibault, G. E. Corazza, and L. Deambrogio, "Random, deterministic, and hybrid algorithms for distributed beamforming," in *Proc. 5th Advanced Satellite and Multimedia Syst. Conf. and the 11th Signal Proc. for Space Comm. Workshop (ASMS/SPSC'10)*, Cagliari, Italy, Sep. 2010, pp. 221–5.

[22] ——, "Phase synchronization algorithms for distributed beamforming with time varying channels in wireless sensor networks," in *Proc. 7th IEEE International Wireless Communications and Mobile Computing Conference (IWCMC'11)*, Istanbul, Turkey, Jul. 2011, pp. 77–82.

[23] K. Zarifi, A. Ghrayeb, and S. Affès, "Distributed beamforming for wireless sensor networks with improved graph connectivity and energy efficiency," *IEEE Trans. on Sig. Proc.*, vol. 58, no. 3, pp. 1904–21, Mar. 2010.

[24] K. Zarifi, S. Affès, and A. Ghrayeb, "Collaborative null-steering beamforming for uniformly distributed wireless sensor networks," *IEEE Trans. on Sig. Proc.*, vol. 58, no. 3, pp. 1889–1903, Mar. 2010.

[25] M. F. A. Ahmed and S. Vorobyov, "Collaborative beamforming for wireless sensor networks with Gaussian distributed sensor nodes," *IEEE Trans. on Wireless Comm.*, vol. 8, no. 2, pp. 638–43, Feb. 2009.

[26] K. Zarifi, S. Affès, and A. Ghrayeb, "Distributed beamforming for wireless sensor networks with random node location," in *Proc. IEEE Int. Conf. Acoustics, Speech and Sig. Processing (ICASSP'09)*, Taipei, Taiwan, Apr. 2009, pp. 2261–4.

[27] K. Hardwick, D. Goeckel, and D. Towsley, "Modeling distributed beamforming in wireless networks," in *Proc. IEEE 46th Annu. Allerton Conference on Comm., Control, and Computing*, Illinois, USA, Sep. 2008, pp. 475–82.

[28] H. Ochiai, P. Mitran, H. V. Poor, and V. Tarokh, "Collaborative beamforming for distributed wireless ad hoc networks," *IEEE Trans. Signal Proc.*, vol. 53, no. 11, pp. 4110–24, Nov. 2005.

[29] M. F. A. Ahmed and S. A. Vorobyov, "Sidelobe control in collaborative beamforming via node selection," *IEEE Trans. on Signal Proc.*, vol. 58, no. 12, pp. 6168–80, Dec. 2010.

[30] M. O. Pun, D. R. Brown, and H. V. Poor, "Opportunistic collaborative beamforming with one-bit feedback," *IEEE Trans. on Wireless Comm.*, vol. 8, no. 5, pp. 2629–41, May 2009.

[31] M. F. A. Ahmed and S. A. Vorobyov, "Node selection for sidelobe control in collaborative beamforming for wireless sensor networks," in *Proc. IEEE 10th Workshop on Sig. Processing Advances in Wireless Comm. (SPAWC'09)*, Perugia, Italy, Jun. 2009, pp. 519–23.

[32] C. W. Chang, A. Kothari, A. Jafri, D. Koutsonikolas, D. Peroulis, and Y. C. Hu, "Radiating sensor selection for distributed beamforming in wireless sensor networks," in *Proc. IEEE Military Comm. Conf. (MILCOM'08)*, San Diego, CA, Nov. 2008, pp. 1–7.

[33] H. Rahul, S. Kumar, and D. Katabi, "JMB: Scaling wireless capacity with user demands," in *Proc. of the ACM Conf. on Applications, Technologies, Architectures, and Protocols for Computer Communication (SIGCOMM'12)*, Helsinki, Finland, Aug. 2012, pp. 235–46.

[34] F. Quitin, U. Madhow, M. Rahman, and R. Mudumbai, "Demonstrating distributed transmit beamforming with software-defined radios," in *Proc. 13th IEEE Int. Symposium on a World of Wireless, Mobile and Multimedia Networks (WoWMoM)'12*, San Francisco, CA, Jun. 2012, pp. 1–3.

[35] L. Berbakov, C. A. Haro, and J. Matamoros, "Distributed beamforming using one bit of feedback: AWGN analysis," in *Proc. 18th European Wireless Conference (EW'12)*, Poznán, Poland, Apr. 2012, pp. 1–4.

[36] R. Mudumbai, G. Barriac, and U. Madhow, "On the feasibility of distributed beamforming in wireless networks," *IEEE Trans. on Wireless Comm.*, vol. 6, no. 5, pp. 1754–63, May 2007.

[37] A. Demir, A. Mehrotra, and J. Roychowdhury, "Phase noise in oscillators: a unifying theory and numerical methods for characterization," *IEEE Trans. on Circuits and Systems I: Fundamental Theory and Applications*, vol. 47, no. 5, pp. 655–74, May 2000.

[38] J. G. Proakis and M. Salehi, *Digital Communications*. Boston: McGraw Hill, 2008.